



Measurement of the dijet invariant mass cross section in $p\bar{p}$ collisions at $\sqrt{s} = 1.96$ TeV

D0 Collaboration

V.M. Abazov^{al}, B. Abbott^{by}, M. Abolins^{bn}, B.S. Acharya^{ae}, M. Adams^{az}, T. Adams^{ax}, E. Aguilo^{f,g}, G.D. Alexeev^{al}, G. Alkhazov^{ap}, A. Alton^{bm,1}, G. Alverson^{bl}, G.A. Alves^b, L.S. Ancu^{ak}, M. Aoki^{ay}, Y. Arnoud^o, M. Arov^{bi}, A. Askew^{ax}, B. Åsman^{aq,ar}, O. Atramentov^{bq}, C. Avilaⁱ, J. BackusMayes^{cf}, F. Badaudⁿ, L. Bagby^{ay}, B. Baldin^{ay}, D.V. Bandurin^{ax}, S. Banerjee^{ae}, E. Barberis^{bl}, A.-F. Barfuss^p, P. Baringer^{bg}, J. Barreto^b, J.F. Bartlett^{ay}, U. Bassler^s, S. Beale^{f,g}, A. Bean^{bg}, M. Begalli^c, M. Begel^{bw}, C. Belanger-Champagne^{aq,ar}, L. Bellantoni^{ay}, J.A. Benitez^{bn}, S.B. Beri^{ac}, G. Bernardi^r, R. Bernhard^x, I. Bertram^{as}, M. Besançon^s, R. Beuselinck^{at}, V.A. Bezzubov^{ao}, P.C. Bhat^{ay}, V. Bhatnagar^{ac}, G. Blazey^{ba}, S. Blessing^{ax}, K. Bloom^{bp}, A. Boehlein^{ay}, D. Boline^{bk}, T.A. Bolton^{bh}, E.E. Boos^{an}, G. Borissov^{as}, T. Bose^{bk}, A. Brandt^{cb}, R. Brock^{bn}, G. Brooijmans^{bt}, A. Bross^{ay}, D. Brown^t, X.B. Bu^h, D. Buchholz^{bb}, M. Buehler^{ce}, V. Buescher^z, V. Bunichev^{an}, S. Burdin^{as,2}, T.H. Burnett^{cf}, C.P. Buszello^{at}, P. Calfayan^{aa}, B. Calpas^p, S. Calvet^q, E. Camacho-Pérez^{ai}, J. Cammin^{bu}, M.A. Carrasco-Lizarraga^{ai}, E. Carrera^{ax}, B.C.K. Casey^{ay}, H. Castilla-Valdez^{ai}, S. Chakrabarti^{bv}, D. Chakraborty^{ba}, K.M. Chan^{be}, A. Chandra^{cd}, G. Chen^{bg}, S. Chevalier-Théry^s, D.K. Cho^{ca}, S.W. Cho^{ag}, S. Choi^{ah}, B. Choudhary^{ad}, T. Christoudias^{at}, S. Cihangir^{ay}, D. Claes^{bp}, J. Clutter^{bg}, M. Cooke^{ay}, W.E. Cooper^{ay}, M. Corcoran^{cd}, F. Couderc^s, M.-C. Cousinou^p, D. Cutts^{ca}, M. Ćwiok^{af}, A. Das^{av}, G. Davies^{at}, K. De^{cb}, S.J. de Jong^{ak}, E. De La Cruz-Burelo^{ai}, K. DeVaughan^{bp}, F. Déliot^s, M. Demarteau^{ay}, R. Demina^{bu}, D. Denisov^{ay}, S.P. Denisov^{ao}, S. Desai^{ay}, H.T. Diehl^{ay}, M. Diesburg^{ay}, A. Dominguez^{bp}, T. Dorland^{cf}, A. Dubey^{ad}, L.V. Dudko^{an}, L. Duflot^q, D. Duggan^{bq}, A. Duperrin^p, S. Dutt^{ac}, A. Dyshkant^{ba}, M. Eads^{bp}, D. Edmunds^{bn}, J. Ellison^{aw}, V.D. Elvira^{ay}, Y. Enari^r, S. Eno^{bj}, H. Evans^{bc}, A. Evdokimov^{bw}, V.N. Evdokimov^{ao}, G. Facini^{bl}, A.V. Ferapontov^{ca}, T. Ferbel^{bj,bu}, F. Fiedler^z, F. Filthaut^{ak}, W. Fisher^{bn}, H.E. Fisk^{ay}, M. Fortner^{ba}, H. Fox^{as}, S. Fuess^{ay}, T. Gadfort^{bw}, A. Garcia-Bellido^{bu}, V. Gavrilov^{am}, P. Gayⁿ, W. Geist^t, W. Geng^{p,bn}, D. Gerbaudo^{br}, C.E. Gerber^{az}, Y. Gershtein^{bq}, D. Gillberg^{f,g}, G. Ginther^{ay,bu}, G. Golovanov^{al}, B. Gómezⁱ, A. Goussiou^{cf}, P.D. Grannis^{bv}, S. Greder^t, H. Greenlee^{ay}, Z.D. Greenwood^{bi}, E.M. Gregores^d, G. Grenier^{u,v}, Ph. Grisⁿ, J.-F. Grivaz^q, A. Grohsjean^s, S. Grünewald^{af}, F. Guo^{bv}, J. Guo^{bv}, G. Gutierrez^{ay}, P. Gutierrez^{by}, A. Haas^{bt,3}, P. Haefner^{aa}, S. Hagopian^{ax}, J. Haley^{bl}, I. Hall^{bn}, L. Han^h, K. Harder^{au}, A. Harel^{bu}, J.M. Hauptman^{bf}, J. Hays^{at}, T. Hebbeker^w, D. Hedin^{ba}, A.P. Heinson^{aw}, U. Heintz^{ca}, C. Hensel^y, I. Heredia-De La Cruz^{ai}, K. Herner^{bm}, G. Hesketh^{bl}, M.D. Hildreth^{be}, R. Hirosky^{ce}, T. Hoang^{ax}, J.D. Hobbs^{bv}, B. Hoeneisen^m, M. Hohlfeld^z, S. Hossain^{by}, P. Houben^{aj}, Y. Hu^{bv}, Z. Hubacek^k, N. Huske^r, V. Hynek^k, I. Iashvili^{bs}, R. Illingworth^{ay}, A.S. Ito^{ay}, S. Jabeen^{ca}, M. Jaffré^q, S. Jain^{bs}, D. Jamin^p, R. Jesik^{at}, K. Johns^{av}, C. Johnson^{bt}, M. Johnson^{ay}, D. Johnston^{bp}, A. Jonckheere^{ay}, P. Jonsson^{at}, A. Juste^{ay,4}, E. Kajfasz^p, D. Karmanov^{an}, P.A. Kasper^{ay}, I. Katsanos^{bp}, R. Kehoe^{cc}, S. Kermiche^p, N. Khalatyan^{ay}, A. Khanov^{bz}, A. Kharchilava^{bs}, Y.N. Kharzeev^{al}, D. Khatidze^{ca}, M.H. Kirby^{bb}, M. Kirsch^w, J.M. Kohli^{ac}, A.V. Kozelov^{ao}, J. Kraus^{bn}, A. Kumar^{bs}, A. Kupco^l, T. Kurča^{u,v}, V.A. Kuzmin^{an}, J. Kvita^j, S. Lammers^{bc}, G. Landsberg^{ca}, P. Lebrun^{u,v}, H.S. Lee^{ag}, W.M. Lee^{ay}, J. Lellouch^r, L. Li^{aw}, Q.Z. Li^{ay}, S.M. Lietti^e, J.K. Lim^{ag}, D. Lincoln^{ay}, J. Linnemann^{bn}, V.V. Lipaev^{ao}, R. Lipton^{ay}, Y. Liu^h, Z. Liu^{f,g}, A. Lobodenko^{ap}, M. Lokajicek^l, P. Love^{as}, H.J. Lubatti^{cf}, R. Luna-Garcia^{ai,5}, A.L. Lyon^{ay}, A.K.A. Maciel^b, D. Mackin^{cd}, R. Magaña-Villalba^{ai}, P.K. Mal^{av}, S. Malik^{bp}, V.L. Malyshev^{al}, Y. Maravin^{bh},

J. Martínez-Ortega ^{ai}, R. McCarthy ^{bv}, C.L. McGivern ^{bg}, M.M. Meijer ^{ak}, A. Melnitchouk ^{bo}, L. Mendoza ⁱ, D. Menezes ^{ba}, P.G. Mercadante ^d, M. Merkin ^{an}, A. Meyer ^w, J. Meyer ^y, N.K. Mondal ^{ae}, T. Moulik ^{bg}, G.S. Muanza ^p, M. Mulhearn ^{ce}, E. Nagy ^p, M. Naimuddin ^{ad}, M. Narain ^{ca}, R. Nayyar ^{ad}, H.A. Neal ^{bm}, J.P. Negret ⁱ, P. Neustroev ^{ap}, H. Nilsen ^x, S.F. Novaes ^e, T. Nunnemann ^{aa}, G. Obrant ^{ap}, D. Onoprienko ^{bh}, J. Orduna ^{ai}, N. Osman ^{at}, J. Osta ^{be}, G.J. Otero y Garzón ^a, M. Owen ^{au}, M. Padilla ^{aw}, M. Pangilinan ^{ca}, N. Parashar ^{bd}, V. Parihar ^{ca}, S.-J. Park ^y, S.K. Park ^{ag}, J. Parsons ^{bt}, R. Partridge ^{ca}, N. Parua ^{bc}, A. Patwa ^{bw}, B. Penning ^{ay}, M. Perfilov ^{an}, K. Peters ^{au}, Y. Peters ^{au}, P. Pétroff ^q, R. Piegaia ^a, J. Piper ^{bn}, M.-A. Pleier ^{bw}, PL.M. Podesta-Lerma ^{ai,6}, V.M. Podstavkov ^{ay}, M.-E. Pol ^b, P. Polozov ^{am}, A.V. Popov ^{ao}, M. Prewitt ^{cd}, D. Price ^{bc}, S. Protopopescu ^{bw}, J. Qian ^{bm}, A. Quadt ^y, B. Quinn ^{bo}, M.S. Rangel ^q, K. Ranjan ^{ad}, P.N. Ratoff ^{as}, I. Razumov ^{ao}, P. Renkel ^{cc}, P. Rich ^{au}, M. Rijssenbeek ^{bv}, I. Ripp-Baudot ^t, F. Rizatdinova ^{bz}, M. Rominsky ^{ay}, C. Royon ^s, P. Rubinov ^{ay}, R. Ruchti ^{be}, G. Safronov ^{am}, G. Sajot ^o, A. Sánchez-Hernández ^{ai}, M.P. Sanders ^{aa}, B. Sanghi ^{ay}, G. Savage ^{ay}, L. Sawyer ^{bi}, T. Scanlon ^{at}, D. Schaile ^{aa}, R.D. Schamberger ^{bv}, Y. Scheglov ^{ap}, H. Schellman ^{bb}, T. Schliephake ^{ab}, S. Schlobohm ^{cf}, C. Schwanenberger ^{au}, R. Schwienhorst ^{bn}, J. Sekaric ^{bg}, H. Severini ^{by}, E. Shabalina ^y, V. Shary ^s, A.A. Shchukin ^{ao}, R.K. Shivpuri ^{ad}, V. Simak ^k, V. Sirotenko ^{ay}, P. Skubic ^{by}, P. Slattery ^{bu}, D. Smirnov ^{be}, G.R. Snow ^{bp}, J. Snow ^{bx}, S. Snyder ^{bw}, S. Söldner-Rembold ^{au}, L. Sonnenschein ^w, A. Sopczak ^{as}, M. Sosebee ^{cb}, K. Soustruznik ^j, B. Spurlock ^{cb}, J. Stark ^o, V. Stolin ^{am}, D.A. Stoyanova ^{ao}, M.A. Strang ^{bs}, E. Strauss ^{bv}, M. Strauss ^{by}, R. Ströhmer ^{aa}, D. Strom ^{az}, L. Stutte ^{ay}, P. Svoisky ^{ak}, M. Takahashi ^{au}, A. Tanasijczuk ^a, W. Taylor ^{f,g}, B. Tiller ^{aa}, M. Titov ^s, V.V. Tokmenin ^{al}, D. Tsybychev ^{bv}, B. Tuchming ^s, C. Tully ^{br}, P.M. Tuts ^{bt}, R. Unalan ^{bn}, L. Uvarov ^{ap}, S. Uvarov ^{ap}, S. Uzunyan ^{ba}, R. Van Kooten ^{bc}, W.M. van Leeuwen ^{aj}, N. Varelas ^{az}, E.W. Varnes ^{av}, I.A. Vasilyev ^{ao}, P. Verdier ^{u,v}, L.S. Vertogradov ^{al}, M. Verzocchi ^{ay}, M. Vesterinen ^{au}, D. Vilanova ^s, P. Vint ^{at}, P. Vokac ^k, H.D. Wahl ^{ax}, M.H.L.S. Wang ^{bu}, J. Warchol ^{be}, G. Watts ^{cf}, M. Wayne ^{be}, G. Weber ^z, M. Weber ^{ay,7}, M. Wetstein ^{bj}, A. White ^{cb}, D. Wicke ^z, M.R.J. Williams ^{as}, G.W. Wilson ^{bg}, S.J. Wimpenny ^{aw}, M. Wobisch ^{bi}, D.R. Wood ^{bl}, T.R. Wyatt ^{au}, Y. Xie ^{ay}, C. Xu ^{bm}, S. Yacoob ^{bb}, R. Yamada ^{ay}, W.-C. Yang ^{au}, T. Yasuda ^{ay}, Y.A. Yatsunenko ^{al}, Z. Ye ^{ay}, H. Yin ^h, K. Yip ^{bw}, H.D. Yoo ^{ca}, S.W. Youn ^{ay}, J. Yu ^{cb}, S. Zelitch ^{ce}, T. Zhao ^{cf}, B. Zhou ^{bm}, J. Zhu ^{bv}, M. Zielinski ^{bu}, D. Ziemińska ^{bc}, L. Zivkovic ^{bt}

^a Universidad de Buenos Aires, Buenos Aires, Argentina^b LAFEX, Centro Brasileiro de Pesquisas Físicas, Rio de Janeiro, Brazil^c Universidade do Estado do Rio de Janeiro, Rio de Janeiro, Brazil^d Universidade Federal do ABC, Santo André, Brazil^e Instituto de Física Teórica, Universidade Estadual Paulista, São Paulo, Brazil^f Simon Fraser University, Burnaby, British Columbia, Canada^g York University, Toronto, Ontario, Canada^h University of Science and Technology of China, Hefei, People's Republic of Chinaⁱ Universidad de los Andes, Bogotá, Colombia^j Center for Particle Physics, Charles University, Faculty of Mathematics and Physics, Prague, Czech Republic^k Czech Technical University in Prague, Prague, Czech Republic^l Center for Particle Physics, Institute of Physics, Academy of Sciences of the Czech Republic, Prague, Czech Republic^m Universidad San Francisco de Quito, Quito, Ecuadorⁿ LPC, Université Blaise Pascal, CNRS/IN2P3, Clermont, France^o LPSC, Université Joseph Fourier Grenoble 1, CNRS/IN2P3, Institut National Polytechnique de Grenoble, Grenoble, France^p CPPM, Aix-Marseille Université, CNRS/IN2P3, Marseille, France^q LAL, Université Paris-Sud, IN2P3/CNRS, Orsay, France^r LPNHE, Universités Paris VI and VII, CNRS/IN2P3, Paris, France^s CEA, Irif, SPP, Saclay, France^t IPHC, Université de Strasbourg, CNRS/IN2P3, Strasbourg, France^u IPNL, Université Lyon 1, CNRS/IN2P3, Villeurbanne, France^v Université de Lyon, Lyon, France^w III. Physikalisches Institut A, RWTH Aachen University, Aachen, Germany^x Physikalisches Institut, Universität Freiburg, Freiburg, Germany^y II. Physikalisches Institut, Georg-August-Universität Göttingen, Göttingen, Germany^z Institut für Physik, Universität Mainz, Mainz, Germany^{aa} Ludwig-Maximilians-Universität München, München, Germany^{ab} Fachbereich Physik, University of Wuppertal, Wuppertal, Germany^{ac} Panjab University, Chandigarh, India^{ad} Delhi University, Delhi, India^{ae} Tata Institute of Fundamental Research, Mumbai, India^{af} University College Dublin, Dublin, Ireland^{ag} Korea Detector Laboratory, Korea University, Seoul, Republic of Korea^{ah} SungKyunKwan University, Suwon, Republic of Korea^{ai} CINVESTAV, Mexico City, Mexico^{aj} FOM-Institute NIKHEF and University of Amsterdam/NIKHEF, Amsterdam, The Netherlands^{ak} Radboud University Nijmegen/NIKHEF, Nijmegen, The Netherlands^{al} Joint Institute for Nuclear Research, Dubna, Russia^{am} Institute for Theoretical and Experimental Physics, Moscow, Russia

^{a1} Moscow State University, Moscow, Russia
^{a2} Institute for High Energy Physics, Protvino, Russia
^{a3} Petersburg Nuclear Physics Institute, St. Petersburg, Russia
^{a4} Stockholm University, Stockholm, Sweden
^{a5} Uppsala University, Uppsala, Sweden
^{a6} Lancaster University, Lancaster LA1 4YB, United Kingdom
^{a7} Imperial College London, London SW7 2AZ, United Kingdom
^{a8} The University of Manchester, Manchester M13 9PL, United Kingdom
^{a9} University of Arizona, Tucson, AZ 85721, USA
^{a10} University of California Riverside, Riverside, CA 92521, USA
^{a11} Florida State University, Tallahassee, FL 32306, USA
^{a12} Fermi National Accelerator Laboratory, Batavia, IL 60510, USA
^{a13} University of Illinois at Chicago, Chicago, IL 60607, USA
^{b1} Northern Illinois University, DeKalb, IL 60115, USA
^{b2} Northwestern University, Evanston, IL 60208, USA
^{b3} Indiana University, Bloomington, IN 47405, USA
^{b4} Purdue University Calumet, Hammond, IN 46323, USA
^{b5} University of Notre Dame, Notre Dame, IN 46556, USA
^{b6} Iowa State University, Ames, IA 50011, USA
^{b7} University of Kansas, Lawrence, KS 66045, USA
^{b8} Kansas State University, Manhattan, KA 66506, USA
^{b9} Louisiana Tech University, Ruston, LA 71272, USA
^{b10} University of Maryland, College Park, MD 20742, USA
^{b11} Boston University, Boston, MA 02215, USA
^{b12} Northeastern University, Boston, MA 02115, USA
^{b13} University of Michigan, Ann Arbor, MI 48109, USA
^{b14} Michigan State University, East Lansing, MI 48824, USA
^{b15} University of Mississippi, University, MS 38677, USA
^{b16} University of Nebraska, Lincoln, NE 68588, USA
^{b17} Rutgers University, Piscataway, NJ 08855, USA
^{b18} Princeton University, Princeton, NJ 08544, USA
^{b19} State University of New York, Buffalo, NY 14260, USA
^{b20} Columbia University, New York, NY 10027, USA
^{b21} University of Rochester, Rochester, NY 14627, USA
^{b22} State University of New York, Stony Brook, NY 11794, USA
^{b23} Brookhaven National Laboratory, Upton, NY 11973, USA
^{b24} Langston University, Langston, OK 73050, USA
^{b25} University of Oklahoma, Norman, OK 73019, USA
^{b26} Oklahoma State University, Stillwater, OK 74078, USA
^{c1} Brown University, Providence, RI 02912, USA
^{c2} University of Texas, Arlington, TX 76019, USA
^{c3} Southern Methodist University, Dallas, TX 75275, USA
^{c4} Rice University, Houston, TX 77005, USA
^{c5} University of Virginia, Charlottesville, VA 22901, USA
^{c6} University of Washington, Seattle, WA 98195, USA

ARTICLE INFO

Article history:

Received 25 February 2010

Received in revised form 9 July 2010

Accepted 7 September 2010

Available online 17 September 2010

Editor: H. Weerts

Keywords:

Quantum chromodynamics

Dijets

Cross section

Tevatron

D0

ABSTRACT

The inclusive dijet production double differential cross section as a function of the dijet invariant mass and of the largest absolute rapidity of the two jets with the largest transverse momentum in an event is measured in $p\bar{p}$ collisions at $\sqrt{s} = 1.96$ TeV using 0.7 fb^{-1} of integrated luminosity collected with the D0 detector at the Fermilab Tevatron Collider. The measurement is performed in six rapidity regions up to a maximum rapidity of 2.4. Next-to-leading order perturbative QCD predictions are found to be in agreement with the data.

© 2010 Elsevier B.V. Open access under CC BY license.

The dominant process contributing to the total inelastic cross section in $p\bar{p}$ collisions at $\sqrt{s} = 1.96$ TeV is the production of

hadronic jets. A measurement of the dijet production cross section as a function of the dijet invariant mass (M_{jj}) can be used to test the predictions of perturbative quantum chromodynamics (QCD), to constrain parton distribution functions (PDFs) of the proton, and to look for signatures of physics not predicted by the standard model. This type of measurement is sensitive to quark compositeness, to extra spatial dimensions, and to undiscovered heavy particles that decay into two quarks [1–8]. The distribution presented in this Letter is particularly sensitive to the PDF of gluons at high proton momentum fraction, a region in which the

¹ Visitor from Augustana College, Sioux Falls, SD, USA.² Visitor from The University of Liverpool, Liverpool, UK.³ Visitor from SLAC, Menlo Park, CA, USA.⁴ Visitor from ICREA/IFAE, Barcelona, Spain.⁵ Visitor from Centro de Investigacion en Computacion - IPN, Mexico City, Mexico.⁶ Visitor from ECFM, Universidad Autonoma de Sinaloa, Culiacán, Mexico.⁷ Visitor from Universität Bern, Bern, Switzerland.

gluon distribution is weakly constrained. Previous measurements of the dijet invariant mass dependent cross section in this energy regime restricted the rapidity of the jets to $|y| < 1.0$ [9–11] where $y = 0.5 \ln[(E + p_L)/(E - p_L)]$, E is the energy of the jet, and p_L is the component of momentum along the direction of the proton beam.

In this Letter, we present a measurement of the double differential dijet production cross section as a function of the dijet invariant mass and the variable $|y|_{\max}$, for $0 < |y|_{\max} < 2.4$. The dijet invariant mass is computed from the four momenta of the two jets with largest transverse momentum (p_T) with respect to the beam direction. Both jets are required to have $p_T > 40$ GeV. The variable $|y|_{\max}$ is defined as $|y|_{\max} = \max(|y_1|, |y_2|)$ where y_1 and y_2 are the rapidities of the two jets with the largest p_T . The cross section results are corrected for instrumental effects and presented at the particle level, which includes energy from stable particles, the underlying event, muons, and neutrinos, as defined in Ref. [12].

This measurement uses approximately 0.7 fb^{-1} of integrated luminosity collected with the D0 detector [13] at the Fermilab Tevatron Collider in $p\bar{p}$ collisions at $\sqrt{s} = 1.96$ TeV during 2004–2005. Outgoing partons created in the scattering process hadronize to produce jets of particles that are detected in the finely segmented liquid-argon and uranium calorimeters which cover most of the solid angle. The central calorimeter (CC) covers the pseudorapidity region $|\eta|$ up to 1.1 ($\eta = -\ln[\tan(\theta/2)]$ where θ is the angle with respect to the proton beam direction) and the two end calorimeters (EC) extend the coverage up to $|\eta| < 4.2$. The intercryostat region (ICR) between the CC and EC contains scintillator-based detectors to improve the energy sampling in this region. Jets are reconstructed by clustering energy deposited in the calorimeter towers using an iterative seed-based cone jet algorithm including midpoints [14] with cone radius $R = \sqrt{(\Delta y)^2 + (\Delta\phi)^2} = 0.7$, where ϕ is the azimuthal angle. The p_T of each jet is calculated using only calorimeter information and the location of the $p\bar{p}$ collision. The measurement is performed in six rapidity regions: $0 < |y|_{\max} \leq 0.4$, $0.4 < |y|_{\max} \leq 0.8$, $0.8 < |y|_{\max} \leq 1.2$, $1.2 < |y|_{\max} \leq 1.6$, $1.6 < |y|_{\max} \leq 2.0$, and $2.0 < |y|_{\max} \leq 2.4$.

Events are required to satisfy jet p_T or dijet invariant mass dependent trigger requirements with minimum dijet invariant mass thresholds. Trigger efficiencies are studied by comparing observables in data sets collected with higher trigger thresholds to those collected using lower trigger thresholds in regions where the lower threshold trigger is 100% efficient. The trigger with the lowest threshold is determined to be 100% efficient in the region of interest by comparing it with a sample of independently triggered muon events. For $|y|_{\max} \leq 1.6$, single jet triggers are used, while dijet invariant mass triggers are used for $|y|_{\max} > 1.6$. The measurement is only done in the kinematic regions where the trigger efficiency is $> 99\%$.

Events must satisfy data and jet quality requirements. The position of the $p\bar{p}$ interaction is reconstructed using a tracking system consisting of silicon microstrip detectors and scintillating fibers located inside a solenoidal magnetic field of approximately 2 T. The position of this primary vertex along the beam line is required to be within 50 cm of the detector center. This requirement is $\approx 93\%$ efficient. Requirements based on calorimeter shower shapes are used to remove the remaining background due to electrons, photons, and detector noise that mimic jets. The sample selection efficiency is $> 99\%$ ($> 97.5\%$ for $0.8 < |y|_{\max} < 1.6$). In order to suppress cosmic ray events, the requirements $\not{E}_T/p_T^{\max} < 0.7$ for $p_T < 100$ GeV of the highest p_T jet and $\not{E}_T/p_T^{\max} < 0.5$ otherwise are applied, where \not{E}_T is the transverse component of the vector sum of the momenta in all calorimeter cells and p_T^{\max} is the transverse momentum of the jet with the maximum p_T . After all these

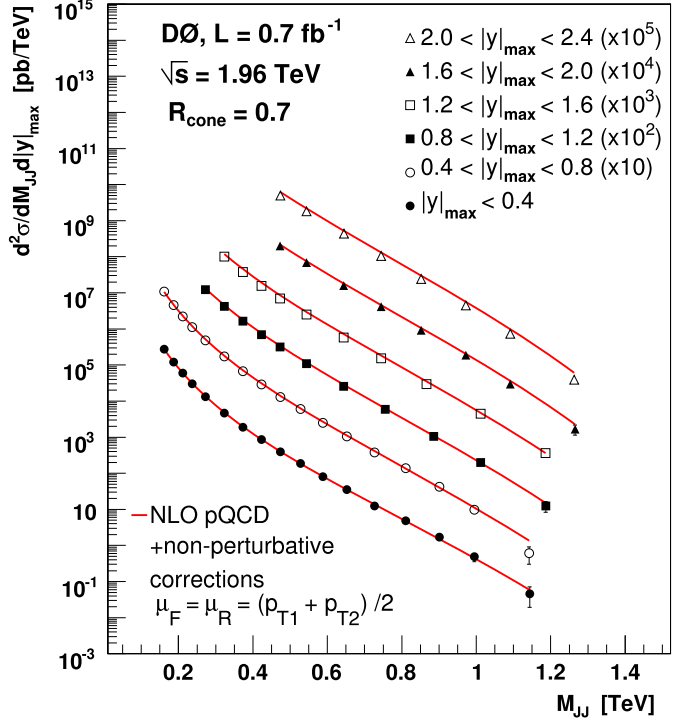


Fig. 1. (Color online.) The dijet production cross section as a function of invariant mass in intervals of $|y|_{\max}$ compared to NLO predictions that include non-perturbative corrections. The uncertainties shown are statistical only.

requirements, the background is reduced to less than 0.1% in our sample.

The measured energy of each jet formed from calorimeter energy depositions is not the same as the actual energy of the particles which enter the calorimeter and shower. The jet four-momentum is corrected, on average, to account for the energy response of the calorimeters, the energy showering in and out of the cone, additional energy from previous beam crossings, and multiple proton–antiproton interactions in the same event. The absolute jet energy calibration correction is determined from the missing transverse energy measured in $\gamma +$ jet events for the region $|\eta| \leq 0.4$, while the rapidity dependence is derived from dijet events using a similar data driven method. Additionally, since this dijet sample has a large fraction of gluon initiated jets, corrections of the order of (2–4)% are made due to the difference in response between quark and gluon initiated jets as estimated using simulated jets produced with the PYTHIA event generator [15] that have been passed through a GEANT-based detector simulation [16]. The total jet energy correction varies between 50% and 20% for a jet p_T of 50 to 400 GeV and adjusts the measured jet energy to the energy of all stable particles that entered the calorimeter except for muons and neutrinos, which are accounted for in the final differential cross section.

Bin sizes in M_{jj} are chosen to be about twice the mass resolution and to correspond to an efficiency and purity of about 50% as determined using a parameterized detector model. The efficiency is defined as the ratio of Monte Carlo (MC) events generated and reconstructed to those generated in an M_{jj} bin, and purity is defined as the ratio of MC events generated and reconstructed in an M_{jj} bin to all events reconstructed in that bin. The detector model used is a fast simulation of the D0 detector based on parameterizations including energy and position resolutions obtained either from the data or from a detailed simulation of the D0 detector using GEANT. This detector model uses events generated by

Table 1

Dijet double differential cross section, $d^2\sigma/dM d|y|_{\max}$, for $|y|_{\max} \leq 0.4$, compared to theoretical predictions with non-perturbative corrections. There is an additional fully correlated uncertainty of 6.1% due to the integrated luminosity determination which is not shown in the table.

Mass range TeV	Central value TeV	Measured cross section pb/TeV	Systematic uncertainty %	Statistical uncertainty %	Theory cross section pb/TeV	Non-perturbative corrections		
						Hadronization	Underlying event	Total
0.150–0.175	0.162	2.74×10^5	+7.3, -6.6	1.9	2.74×10^5	0.917	1.180	1.082
0.175–0.200	0.187	1.22×10^5	+7.3, -6.6	2.6	1.22×10^5	0.930	1.147	1.066
0.200–0.225	0.212	6.00×10^4	+7.3, -6.6	1.4	5.93×10^4	0.939	1.125	1.056
0.225–0.250	0.237	3.02×10^4	+7.3, -6.6	1.8	3.10×10^4	0.945	1.110	1.049
0.250–0.300	0.272	1.32×10^4	+7.3, -6.6	1.3	1.36×10^4	0.950	1.095	1.041
0.300–0.350	0.323	4.69×10^3	+7.5, -6.8	1.6	4.85×10^3	0.955	1.083	1.035
0.350–0.400	0.373	1.90×10^3	+7.3, -6.7	1.3	1.96×10^3	0.959	1.075	1.030
0.400–0.450	0.423	8.48×10^2	+7.4, -6.8	1.4	8.60×10^2	0.961	1.069	1.027
0.450–0.500	0.473	3.93×10^2	+7.6, -7.1	1.7	4.01×10^2	0.963	1.065	1.025
0.500–0.560	0.528	1.84×10^2	+7.9, -7.4	2.1	1.85×10^2	0.965	1.058	1.022
0.560–0.620	0.588	7.93×10^1	+8.3, -8.0	3.1	8.17×10^1	0.967	1.054	1.019
0.620–0.690	0.652	3.50×10^1	+9.1, -8.8	4.2	3.53×10^1	0.966	1.056	1.020
0.690–0.770	0.727	1.23×10^1	+10.4, -10.0	6.5	1.37×10^1	0.967	1.054	1.019
0.770–0.860	0.811	4.83×10^0	+12.1, -11.7	9.8	4.77×10^0	0.968	1.052	1.018
0.860–0.950	0.901	1.69×10^0	+14.3, -13.7	15.8	1.52×10^0	0.968	1.050	1.017
0.950–1.050	0.995	4.95×10^{-1}	+16.7, -15.8	31.6	4.49×10^{-1}	0.969	1.049	1.016
1.050–1.300	1.144	4.56×10^{-2}	+22.1, -20.0	57.7	5.83×10^{-2}	0.970	1.047	1.015

Table 2

Dijet double differential cross section, $d^2\sigma/dM d|y|_{\max}$, for $0.4 < |y|_{\max} < 0.8$, compared to theoretical predictions with non-perturbative corrections. There is an additional fully correlated uncertainty of 6.1% due to the integrated luminosity determination which is not shown in the table.

Mass range TeV	Central value TeV	Measured cross section pb/TeV	Systematic uncertainty %	Statistical uncertainty %	Theory cross section pb/TeV	Non-perturbative corrections		
						Hadronization	Underlying event	Total
0.150–0.175	0.162	1.08×10^6	+7.4, -7.4	1.3	1.07×10^6	0.946	1.127	1.066
0.175–0.200	0.187	4.67×10^5	+7.5, -7.4	1.6	4.73×10^5	0.951	1.109	1.055
0.200–0.225	0.212	2.24×10^5	+7.5, -7.5	1.1	2.29×10^5	0.955	1.094	1.045
0.225–0.250	0.237	1.14×10^5	+7.6, -7.5	1.2	1.19×10^5	0.958	1.084	1.040
0.250–0.300	0.272	4.91×10^4	+7.9, -7.8	1.1	5.14×10^4	0.960	1.077	1.034
0.300–0.350	0.323	1.74×10^4	+7.6, -7.6	1.2	1.81×10^4	0.961	1.072	1.030
0.350–0.400	0.373	6.77×10^3	+7.9, -7.7	1.1	7.15×10^3	0.963	1.067	1.028
0.400–0.450	0.423	2.89×10^3	+8.0, -7.9	1.2	3.07×10^3	0.964	1.064	1.025
0.450–0.500	0.473	1.28×10^3	+8.3, -8.2	1.3	1.40×10^3	0.964	1.061	1.023
0.500–0.560	0.528	5.97×10^2	+8.7, -8.6	1.4	6.25×10^2	0.965	1.058	1.021
0.560–0.620	0.589	2.50×10^2	+9.4, -9.2	1.9	2.68×10^2	0.966	1.056	1.020
0.620–0.690	0.652	1.04×10^2	+10.3, -10.1	2.5	1.11×10^2	0.966	1.054	1.018
0.690–0.770	0.726	3.78×10^1	+11.7, -11.3	3.8	4.12×10^1	0.967	1.052	1.017
0.770–0.860	0.811	1.38×10^1	+13.5, -13.0	5.7	1.35×10^1	0.967	1.050	1.016
0.860–0.950	0.901	4.20×10^0	+15.7, -14.9	10.7	4.08×10^0	0.968	1.047	1.014
0.950–1.050	0.994	9.90×10^{-1}	+18.4, -17.0	20.4	1.13×10^0	0.969	1.045	1.012
1.050–1.300	1.142	6.08×10^{-2}	+23.5, -20.9	50.0	1.36×10^{-1}	0.969	1.045	1.012

PYTHIA (using the settings of Tune QW [17] and MSTW2008LO PDFs [18]) that have been reweighted to match measured dijet invariant mass and rapidity distributions in data. This reweighting assumes a smooth underlying distribution, which does not include resonances. After this tuning, other spectra fundamental to this measurement, such as the jet p_T distributions, show good agreement between the data and simulation. Because the underlying dijet cross sections are steeply falling, the measured dijet invariant mass distributions are systematically shifted to higher invariant mass values due to jet p_T resolution. The jet p_T resolution is measured in data using momentum conservation in the transverse plane for events with exactly two jets, and is found to be approximately 13% (7%) at $p_T \approx 50$ (400) GeV in the CC and EC, and 16% (11%) at $p_T \approx 50$ (400) GeV in the ICR. The bin-to-bin migrations due to experimental resolution are determined using the parametrized detector model. To minimize migrations between M_{jj} bins due to resolution effects, we use the simulation to obtain a rescaling function in M_{jj} that optimizes the corre-

lation between the reconstructed and true values. The total experimental corrections to the data are less than $\pm 2\%$ across the whole dijet invariant mass range for $|y|_{\max} < 0.8$, vary from 0.5% at $M_{jj} = 0.4$ TeV to 22% at 1.2 TeV for $0.8 < |y|_{\max} < 1.6$, and from 1% at $M_{jj} = 0.4$ TeV to 11% at 1.3 TeV for $1.6 < |y|_{\max} < 2.4$.

We compute the doubly differential dijet cross section as a function of dijet invariant mass and $|y|_{\max}$ corrected for all selection efficiencies and migrations due to resolution, and for the energies of minimum ionizing muons and non-interacting neutrinos associated with the jet as determined from our detector simulation. The result is plotted in all six rapidity regions in Fig. 1 and tabulated in Tables 1–6. The quoted central value of M_{jj} in each bin is the location where the differential cross section has the same value as the bin average [19].

The systematic uncertainties on the cross section are dominated by the uncertainties in the jet energy calibration, which range from 6% to 22% in the CC, from 8% to 30% in the ICR, and from 15% to

Table 3

Dijet double differential cross section, $d^2\sigma/dM d|y|_{\max}$, for $0.8 < |y|_{\max} \leq 1.2$, compared to theoretical predictions with non-perturbative corrections. There is an additional fully correlated uncertainty of 6.1% due to the integrated luminosity determination which is not shown in the table.

Mass range TeV	Central value TeV	Measured cross section pb/TeV	Systematic uncertainty %	Statistical uncertainty %	Theory cross section pb/TeV	Non-perturbative corrections		
						Hadronization	Underlying event	Total
0.250–0.300	0.272	1.21×10^5	+10.3, -10.0	1.1	1.34×10^5	0.949	1.126	1.069
0.300–0.350	0.323	4.18×10^4	+9.7, -9.5	1.3	4.63×10^4	0.953	1.111	1.059
0.350–0.400	0.373	1.63×10^4	+9.4, -9.1	1.7	1.80×10^4	0.956	1.100	1.052
0.400–0.450	0.423	6.86×10^3	+9.3, -9.0	1.4	7.55×10^3	0.958	1.092	1.046
0.450–0.500	0.473	3.10×10^3	+9.3, -9.0	1.9	3.38×10^3	0.960	1.083	1.041
0.500–0.600	0.544	1.07×10^3	+9.6, -9.3	1.2	1.17×10^3	0.963	1.076	1.035
0.600–0.700	0.644	2.57×10^2	+10.6, -10.4	1.8	2.83×10^2	0.964	1.070	1.031
0.700–0.830	0.756	5.95×10^1	+12.7, -12.6	2.5	6.30×10^1	0.965	1.065	1.028
0.830–0.960	0.886	1.08×10^1	+16.4, -16.0	5.4	1.10×10^1	0.966	1.062	1.026
0.960–1.080	1.012	2.10×10^0	+20.6, -19.7	12.5	1.95×10^0	0.967	1.058	1.023
1.080–1.400	1.186	1.43×10^{-1}	+28.5, -24.5	28.9	1.50×10^{-1}	0.969	1.053	1.020

Table 4

Dijet double differential cross section, $d^2\sigma/dM d|y|_{\max}$, for $1.2 < |y|_{\max} \leq 1.6$, compared to theoretical predictions with non-perturbative corrections. There is an additional fully correlated uncertainty of 6.1% due to the integrated luminosity determination which is not shown in the table.

Mass range TeV	Central value TeV	Measured cross section pb/TeV	Systematic uncertainty %	Statistical uncertainty %	Theory cross section pb/TeV	Non-perturbative corrections		
						Hadronization	Underlying event	Total
0.300–0.350	0.323	1.00×10^5	+10.7, -10.4	1.2	1.19×10^5	0.949	1.143	1.085
0.350–0.400	0.373	3.79×10^4	+10.4, -10.1	1.3	4.60×10^4	0.951	1.133	1.077
0.400–0.450	0.423	1.61×10^4	+10.4, -9.9	1.7	1.91×10^4	0.952	1.125	1.071
0.450–0.500	0.473	7.11×10^3	+10.7, -10.0	2.3	8.60×10^3	0.954	1.116	1.065
0.500–0.600	0.544	2.54×10^3	+11.3, -10.4	1.6	2.97×10^3	0.955	1.109	1.059
0.600–0.700	0.644	5.94×10^2	+12.3, -11.7	1.3	7.16×10^2	0.956	1.103	1.055
0.700–0.800	0.744	1.58×10^2	+14.1, -13.4	2.1	1.84×10^2	0.957	1.098	1.051
0.800–0.960	0.866	3.16×10^1	+17.8, -16.8	2.9	3.57×10^1	0.958	1.095	1.048
0.960–1.080	1.012	5.08×10^0	+22.7, -21.4	8.0	4.78×10^0	0.958	1.091	1.045
1.080–1.400	1.186	4.77×10^{-1}	+29.5, -27.9	15.8	3.67×10^{-1}	0.959	1.084	1.040

Table 5

Dijet double differential cross section, $d^2\sigma/dM d|y|_{\max}$, for $1.6 < |y|_{\max} \leq 2.0$, compared to theoretical predictions with non-perturbative corrections. There is an additional fully correlated uncertainty of 6.1% due to the integrated luminosity determination which is not shown in the table.

Mass range TeV	Central value TeV	Measured cross section pb/TeV	Systematic uncertainty %	Statistical uncertainty %	Theory cross section pb/TeV	Non-perturbative corrections		
						Hadronization	Underlying event	Total
0.450–0.500	0.473	2.01×10^4	+12.0, -13.5	2.2	2.27×10^4	0.940	1.151	1.083
0.500–0.600	0.544	6.88×10^3	+13.8, -14.6	2.3	7.82×10^3	0.940	1.141	1.073
0.600–0.700	0.644	1.58×10^3	+16.3, -17.3	3.2	1.87×10^3	0.941	1.132	1.065
0.700–0.800	0.744	4.10×10^2	+19.9, -18.7	2.3	4.74×10^2	0.941	1.125	1.058
0.800–0.920	0.852	9.30×10^1	+21.1, -17.0	2.8	1.10×10^2	0.941	1.119	1.054
0.920–1.040	0.972	1.93×10^1	+27.1, -20.3	4.9	2.16×10^1	0.941	1.112	1.047
1.040–1.160	1.092	3.15×10^0	+32.5, -24.3	11.2	3.68×10^0	0.942	1.104	1.040
1.160–1.500	1.266	1.92×10^{-1}	+36.3, -33.4	25.1	2.34×10^{-1}	0.942	1.100	1.037

45% in the EC region. The second largest systematic uncertainty comes from the p_T resolution uncertainty, which ranges between 2% and 10% in all regions. The luminosity determination has an uncertainty of 6.1%, which is completely correlated across all bins. The systematic uncertainties on the jet identification efficiency corrections, corrections due to misvertexing and angular resolutions, and MC reweighting are calculated using the parameterized model of the detector and affect the measured cross section by less than 2% in all regions.

The data are compared to the next-to-leading order (NLO) prediction computed using fastNLO [20] based on NLOJET++ [21,22] for MSTW2008NILO PDFs with $\alpha_s(M_Z) = 0.120$. The NLO prediction is corrected for hadronization and underlying event effects using corrections which range between -10% and $+23\%$ depending on the mass in all rapidity regions. The correction factors are obtained

by turning these effects on and off individually in PYTHIA. The uncertainty due to the non-perturbative corrections is estimated as 50% of the individual corrections, with the uncertainty determined by adding the individual contributions in quadrature. The renormalization and factorization scales are set to $\mu_R = \mu_F = p_T = (p_{T1} + p_{T2})/2$ where p_{T1} and p_{T2} are the p_T of the two highest p_T jets. The effect of varying these scales simultaneously from $\mu = p_T/2$ to $\mu = 2p_T$ is shown in Fig. 2 where the ratio of data to theory is plotted.

The experimental uncertainties are similar in size to both the PDF and the scale uncertainties, suggesting that the measurement will constrain theoretical models. We are quoting PDF uncertainties corresponding to a 90% C.L. The total uncertainties are smaller than those of earlier measurements at this same center-of-mass energy [11]. In addition to comparing the D0 measurement to the theo-

Table 6

Dijet double differential cross section, $d^2\sigma/dM d|y|_{\max}$, for $2.0 < |y|_{\max} \leq 2.4$, compared to theoretical predictions with non-perturbative corrections. There is an additional fully correlated uncertainty of 6.1% due to the integrated luminosity determination which is not shown in the table.

Mass range TeV	Central value TeV	Measured cross section pb/TeV	Systematic uncertainty %	Statistical uncertainty %	Theory cross section pb/TeV	Non-perturbative corrections		
						Hadronization	Underlying event	Total
0.450–0.500	0.473	4.95×10^4	+16.1, –13.7	2.1	6.08×10^4	0.928	1.229	1.141
0.500–0.600	0.544	1.81×10^4	+16.2, –14.1	2.1	2.15×10^4	0.925	1.222	1.130
0.600–0.700	0.644	4.36×10^3	+16.5, –15.2	2.5	5.21×10^3	0.923	1.216	1.122
0.700–0.800	0.744	1.02×10^3	+17.4, –17.0	2.1	1.31×10^3	0.920	1.211	1.115
0.800–0.920	0.852	2.37×10^2	+20.0, –19.9	2.4	2.998×10^2	0.919	1.208	1.110
0.920–1.040	0.972	4.43×10^1	+24.8, –23.9	3.5	5.66×10^1	0.917	1.203	1.103
1.040–1.160	1.091	7.25×10^0	+33.0, –28.0	7.3	9.86×10^0	0.915	1.198	1.095
1.160–1.500	1.263	4.12×10^{-1}	+46.1, –33.8	16.5	6.09×10^{-1}	0.913	1.195	1.092

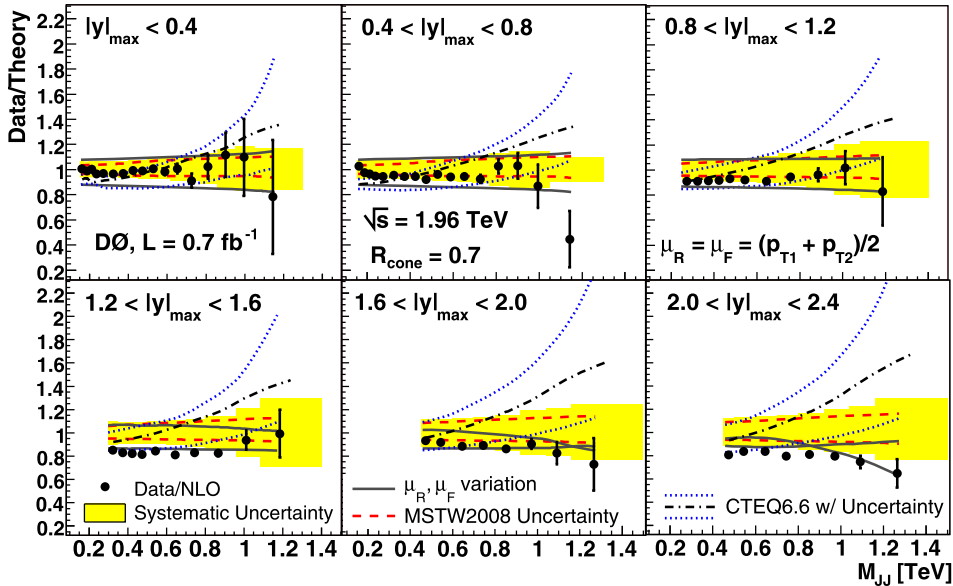


Fig. 2. (Color online.) Ratio of data over theoretical expectation using MSTW2008NLO PDFs in all six $|y|_{\max}$ bins. The measurement systematic uncertainty is shown as a shaded band. There is an additional fully correlated uncertainty of 6.1% due to the integrated luminosity determination which is not shown in the plots. The legend for all six plots shown is spread out over the three bottom plots with other relevant information in the top three plots. PDF uncertainties show a 90% C.L. band.

retical predictions using MSTW2008NLO PDFs, we also compare to the theoretical predictions using CTEQ6.6 PDFs [23]. The difference in the cross section due to the choice of PDFs is (40–60)% at the highest mass. Although the central value for the MSTW2008NLO PDFs are favored, it is important to note that their determination included a measurement of the D0 inclusive jet production cross section [24] which is based on the same dataset as the present measurement. In addition, these PDFs exclude Tevatron data taken before 2000, while the CTEQ6.6 PDFs include that data and do not include Tevatron data taken after 2000.

In summary, we have presented a new measurement of the dijet production cross section as a function of the dijet invariant mass and of the largest rapidity of the two highest p_T jets that extends the rapidity range beyond previous measurements, with systematic uncertainties that are significantly smaller. In general, the data are described by NLO QCD predictions using MSTW2008NLO or CTEQ6.6 PDFs in all rapidity regions, though the central value of the CTEQ6.6 PDFs differs from the data for high dijet mass at larger rapidities.

Acknowledgements

We thank the staffs at Fermilab and collaborating institutions, and acknowledge support from the DOE and NSF (USA); CEA

and CNRS/IN2P3 (France); FASI, Rosatom and RFBR (Russia); CNPq, FAPERJ, FAPESP and FUNDUNESP (Brazil); DAE and DST (India); Colciencias (Colombia); CONACYT (Mexico); KRF and KOSEF (Korea); CONICET and UBACyT (Argentina); FOM (The Netherlands); STFC and the Royal Society (United Kingdom); MSMT and GACR (Czech Republic); CRC Program and NSERC (Canada); BMBF and DFG (Germany); SFI (Ireland); The Swedish Research Council (Sweden); and CAS and CNSF (China).

Appendix A. Supplementary material

Supplementary material related to this article can be found online at doi:10.1016/j.physletb.2010.09.013.

References

- [1] E. Eichten, K. Lane, M.E. Peskin, Phys. Rev. Lett. 50 (1983) 811.
- [2] E. Eichten, I. Hinchliffe, K. Lane, C. Quigg, Rev. Modern Phys. 56 (1984) 579; E. Eichten, I. Hinchliffe, K. Lane, C. Quigg, Rev. Modern Phys. 58 (1986) 1065 (Addendum).
- [3] K. Lane, arXiv:hep-ph/9605257.
- [4] N. Arkani-Hamed, S. Dimopoulos, G.R. Dvali, Phys. Lett. B 429 (1998) 263.
- [5] D. Atwood, S. Bar-Shalom, A. Soni, Phys. Rev. D 62 (2000) 056008.
- [6] K.R. Dienes, E. Dudas, T. Gherghetta, Nucl. Phys. B 537 (1999) 47.
- [7] A. Pomarol, M. Quiros, Phys. Lett. B 438 (1998) 255.
- [8] K. Cheung, G. Landsberg, Phys. Rev. D 65 (2002) 076003.

- [9] B. Abbott, et al., D0 Collaboration, Phys. Rev. D 64 (2001) 032003.
- [10] B. Abbott, et al., D0 Collaboration, Phys. Rev. Lett. 82 (1999) 2457.
- [11] T. Aaltonen, et al., CDF Collaboration, Phys. Rev. D 29 (2009) 112002.
- [12] C. Buttar, et al., arXiv:0803.0678 [hep-ph].
- [13] V.M. Abazov, et al., D0 Collaboration, Nucl. Instrum. Methods Phys. Res. A 565 (2006) 463.
- [14] G.C. Blazey, et al., in: U. Baur, R.K. Ellis, D. Zeppenfeld (Eds.), Proceedings of the Workshop: QCD and Weak Boson Physics in Run II, Fermilab-Pub-00/297, 2000.
- [15] T. Sjöstrand, et al., Comput. Phys. Comm. 135 (2001) 238.
- [16] R. Brun, F. Carminati, CERN Program Library Long Writeup Report No. W5013, 1993, unpublished.
- [17] M.G. Albrow, et al., TeV4LHC QCD Working Group, arXiv:hep-ph/0610012.
- [18] A.D. Martin, W.J. Stirling, R. S Thorne, G. Watt, Eur. Phys. J. C 63 (2009) 189.
- [19] G.D. Lafferty, T.R. Wyatt, Nucl. Instrum. Methods A 355 (1995) 541.
- [20] T. Kluge, K. Rabbertz, M. Wobisch, arXiv:hep-ph/0609285.
- [21] Z. Nagy, Phys. Rev. D 68 (2003) 094002.
- [22] Z. Nagy, Phys. Rev. Lett. 88 (2002) 122003.
- [23] P.M. Nadolsky, et al., Phys. Rev. D 78 (2008) 013004.
- [24] V.M. Abazov, et al., Phys. Rev. Lett. 101 (2008) 062001.